MICROBIOLOGY

# Efflux pumps control intracellular drug-target kinetics by limiting rebinding in bacteria

**Subrata Dev[1]†‡, Keiran Stevenson[1]†, Dai Le[1]†§, Minsu Kim[1,2,3]***



**Bacterial efflux pumps are major contributors to multidrug resistance, classically described as "gatekeepers" that reduce drug entry. Here, we uncover a post–entry mechanism of efflux pumps, revealing their function deep into intracellular drug-target interactions. Using quantitative live-cell imaging, we monitored the activity of major efflux systems in *Escherichia coli* and *Pseudomonas aeruginosa* with Hoechst 33342 (HCT), a DNA binding inhibitor. We found that inactivation of efflux (Δ*tolC* in *E. coli* and Δ6 in *P. aeruginosa*) increased the apparent HCT-DNA affinity, mediated by a decreased apparent unbinding rate, whereas the intrinsic rate remained unchanged. Statistical physics modeling and experimental testing show that, unlike under dilute in vitro conditions, drug molecules that unbind from their targets in intracellular environments undergo successive rebinding, prolonging the total lifetime of the drug bound to the target. However, efflux pumps counteract this effect by suppressing rebinding, thereby kinetically destabilizing drug-target interactions. This biophysical mechanism acts multiplicatively with the canonical gatekeeping effect to broaden and amplify drug resistance.**

## INTRODUCTION

Antibiotic resistance is an increasingly serious threat to public health as existing antibiotics lose their potency and become clinically ineffective (*1*). This challenge is further compounded by the slow pace of new drug development. Most antibiotics act by binding to intracellular macromolecules, thereby disrupting cellular functions. Resistance can arise through genetic mutations that alter the structure of either the drug or its target, reducing binding affinity and diminishing antibiotic efficacy (*2*).

Recently, efflux pumps have been recognized as major contributors to multidrug resistance (*3*). Ubiquitous across bacterial species, these transporters underlie a broad spectrum of innate resistance to antibiotics (*4*). In addition, their activities provide a temporal window for bacteria to mutate and acquire additional resistance genetically (*5*). As such, understanding the mechanistic basis of efflux pump function is critical for developing new strategies to counter antibiotic resistance.

It is widely accepted that efflux pumps act as permeation barriers (*4*). Embedded in the cell membrane, they capture drug molecules and expel them into extracellular space. Efflux pumps are classified into five superfamilies, based on their molecular characteristics (*6*). Among them, the resistance-nodulation-division (RND) family plays a particularly important role in drug resistance due to its broad substrate specificity, extruding a wide range of structurally diverse drugs (*7*). The up-regulation of RND pumps is common among clinical isolates and is strongly associated with multidrug resistance (*8*).

The AcrAB-TolC system in *Escherichia coli* has served as a primary model for studying RND efflux pumps (*9*). Typical of RND pumps, it forms a tripartite complex composed of the outer membrane channel (TolC), the inner membrane transporter (AcrB), and the periplasmic adaptor protein (AcrA), thereby spanning the entire cell envelope. Ongoing studies suggest that the periplasmic domain of this complex is critical for substrate recognition and binding (*10*–*12*), favoring a view is that AcrAB-TolC captures substrates from the periplasmic space (or the outer leaflet of the inner membrane) and expel them directly (*13*, *14*). In this way, when extracellular drug molecules enter the periplasm, they are intercepted at the cell envelope reaching intracellular targets, effectively lowering their cytoplasmic accumulation. We refer to this barrier function as gatekeeping. The AcrAB-TolC system is widespread in Gram-negative species, including many pathogens (*15*). Given its central role in drug resistance, several inhibitors are under investigation to block its activity and restore the efficacy of existing antibiotics (*16*).

However, efflux pumps do not completely prevent drug molecules from reaching their intracellular targets. As external drug concentrations increase, more molecules bypass the membrane-bound pumps and accumulate in the cytoplasm, where they interact with intended targets.

In the past, drug-target interactions were extensively studied to predict the cytotoxic effects of drugs. Binding affinity is computationally modeled on the basis of chemical structure and thermodynamics and tested in vitro using purified targets (*17*, *18*). These measurements have guided medicinal chemistry efforts to optimize drug molecules for higher affinity. In recent years, the mean lifetime of drug-target complexes, quantified as the inverse of the unbinding rate $k_{off}$, emerged as an additional key determinant of cytotoxicity (*19*–*21*). The complex lifetime matters because a drug molecule is active only when it is bound to its target. In the past, however, drug-target interactions were mostly studied in vitro. These studies do not fully capture the spatial and temporal dynamics of interactions within the native environment, i.e., within cells (*22*).

In this study, we investigated drug-target interactions in live bacterial cells, with a particular focus on the role of efflux pumps. To probe these dynamics, we used benzimidazole, one of the most common structural motifs in Food and Drug Administration–approved drugs (*23*, *24*). Because of its strong affinity for nucleotide bases, it is being widely adopted in medicinal chemistry to develop antimicrobials, antiviral, anticancer, and anti-inflammatory agents (*25*, *26*).

Among these compounds, a benzimidazole derivative known as Hoechst 33342 (HCT) (*27*) exhibits physicochemical properties of drug molecules. It has a molecular weight (562 Da) and lipophilicity

[1]Department of Physics, Emory University, Atlanta, GA 30322, USA. [2]Graduate Division of Biological and Biomedical Sciences, Emory University, Atlanta, GA 30322, USA. [3]Antibiotic Research Center, Emory University, Atlanta, GA 30322, USA.
*Corresponding author. Email: minsu.kim@emory.edu
†These authors contributed equally to this work.
‡Present address: Prescience Insilico, Bengaluru, Karnataka, India.
§Present address: Department of Computer Science, Texas A&M University, College Station, TX 78412, USA.

[logP ≈ 2.7, based on SwissADME (*28*)] typical of orally active small-molecule drugs (*29*–*31*). It is weakly basic at physiological pH (*32*). These properties allow HCT to cross the lipid membranes and accumulate in the cytoplasm, where it binds specifically to DNA and inhibits replication and gene expression (*33*). Notably, many of these chemical properties are also recognized by efflux systems (*34*). As such, HCT has been widely used as a functional reporter of efflux pump activity across different bacterial species (*35*).

HCT's fluorescence provides a robust method for studying drug-target interactions quantitatively (*36*, *37*). It fluoresces upon binding to DNA and loses fluorescence upon unbinding. We previously showed that spatial HCT intensity profiles match the spatial intensity profile of DNA binding fluorescent proteins, demonstrating that HCT fluorescence inside the cell results primarily from its binding to DNA (*38*), in agreement with an earlier biochemical study (*27*). Therefore, HCT-DNA interactions provide a useful and tractable model for investigating drug-target binding and unbinding dynamics inside live bacterial cells.

In this study, we leveraged these properties of HCT and expanded the finding using physics-based modeling to analyze drug-target interactions inside intact cells, which shows that the effects of efflux pumps go beyond gatekeeping. First, we quantified the intracellular HCT-DNA bound state by measuring HCT fluorescence intensity in *E. coli*. We exposed efflux-deficient (Δ*tolC*) cells to a different external HCT concentration than that used for wild-type (WT) cells to equalize the intracellular level of HCT-DNA complexes across strains. The resulting concentration difference could not be explained by the gatekeeping role of efflux pumps alone, instead pointing to different intracellular drug-target kinetic and/or equilibrium constants between the efflux-active and efflux-deficient strains. Our additional experiments confirmed that the efflux pumps markedly alter the apparent binding affinity, $K_D$, by modulating the unbinding rate $k_{off}$. This was unexpected, given that efflux pumps are localized to the membrane and physically distant from HCT's cytoplasmic target, DNA. To explain how efflux pumps remotely act to modulate cytoplasmic drug-target interactions, we used a statistical mechanics model of partially reflected Brownian motion, which reveals a kinetic competition between intracellular diffusion and outward permeation of drug molecules. Computational simulations showed that drug molecules, upon dissociating from their targets, often rebind. Efflux pumps facilitate their export and reduce the likelihood of rebinding, thereby altering the apparent drug-target affinity and unbinding rate without affecting the drug-target thermodynamic stability. We validated this prediction experimentally by measuring HCT-DNA rebinding in both *E. coli* and *Pseudomonas aeruginosa*, another species known for its high efflux activity. Analyzing the diffusion constants and membrane permeability of small-molecule drugs in our model suggests that this long-range kinetic mechanism is applicable to a wide range of drug molecules. Coupled with the broad substrate specificity of efflux pumps—particularly those of the RND family (*7*)—this finding provides physical insights into how efflux pumps function to restrict drugs' access to their intracellular targets and drive multidrug resistance.

## RESULTS

### Efflux pumps reduce intracellular HCT accumulation

We exposed WT *E. coli* to a range of external HCT concentrations and imaged the cells using fluorescence microscopy. Increasing external HCT concentrations led to higher intracellular fluorescence, with the relationship remaining linear at lower doses (fig. S1). However, beyond 10 μM, further increases in external HCT resulted in minimal changes in intracellular fluorescence, indicating that its target (DNA) is nearly saturated.

To avoid this saturation regime, we used 1 μM HCT for WT cells in subsequent experiments. To characterize the temporal accumulation of HCT on its target (DNA), we measured fluorescence intensity $F(t)$ at various time points after HCT addition (time zero). As shown in Fig. 1A, $F(t)$ increased initially over time and reached a steady-state plateau, denoted as $F_s$.

To test whether HCT is a substrate of the AcrAB-TolC efflux pump, we analyzed strains lacking *acrA*, *acrB*, or *tolC*. All knockout strains showed substantially elevated $F_s$ compared to WT (fig. S2), indicating that HCT is a substrate for the AcrAB-TolC system, consistent with previous studies (*35*, *39*, *40*). As discussed above, the current molecular understanding of this system (*13*, *14*) suggests that it likely captures HCT in the periplasmic space or in the periplasmic leaflet of the inner membrane, extruding it to the extracellular medium. Deletion of any single component—*acrA*, *acrB*, or *tolC*—was sufficient to increase $F_s$. On the basis of this, we used the Δ*tolC* strain for all subsequent experiments.

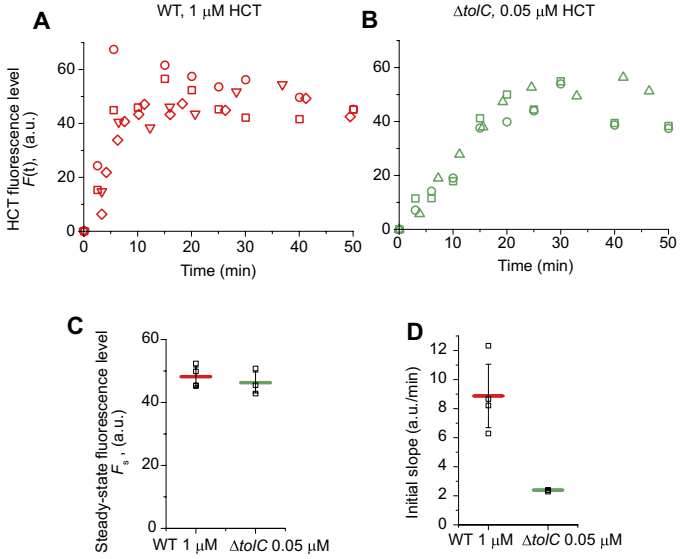


**Fig. 1. Intracellular HCT fluorescence intensity in live *E. coli* cells.** (**A** and **B**) After addition of HCT (time zero), the intracellular fluorescence intensity, $F(t)$, increased and reached a steady-state level, $F_s$. In Δ*tolC* cells, 0.05 μM HCT achieved the same $F_s$ as 1 μM in WT, indicating the same number of DNA-bound HCT molecules (whereas unbound pools may differ; see fig. S13). Three independent replicates were performed; different symbols represent different replicates. At least 30 cells were analyzed in each replicate. a.u., arbitrary units. (**C**) Data points between 20 and 50 min were averaged to quantify the steady-state fluorescence level, $F_s$. We estimate that the observed $F_s$ corresponds to bound HCT (~70 μM), occupying ~10% of available sites (see Supplementary Text, section 5). Open squares represent individual values from independent replicates. A two-tailed *t* test (with two-sample unequal variance) comparing $F_s$ between WT and Δ*tolC* strains yielded $P = 0.556$, indicating no significant difference. (**D**) Data points between 0 and 6 min for WT and 0 and 15 min for Δ*tolC* were fit with linear regression to calculate the initial rate of increase. A two-tailed *t* test (with two-sample unequal variance) comparing the slopes between WT and Δ*tolC* yielded $P = 0.014$, indicating a substantial difference in the slope.

### Reduction in drug permeation by efflux pumps alone is not sufficient to explain their effects on intracellular HCT levels

When studying the efflux activity, it is typical to compare the responses of efflux-active and efflux-deficient strains to the same drug concentration. However, at 1 μM HCT, the steady-state fluorescence intensity ($F_s$) in the Δ*tolC* strain reached a level close to the target saturation (fig. S2)—a regime we deliberately avoided in the WT (fig. S1). This implies that, at the same external concentration, the two strains experience distinct intracellular drug regimes, complicating direct comparison.

This discrepancy introduces additional complications. Given the inhibitory effects of HCT on gene expression and DNA replication (*33*), increased HCT binding is expected to slow cell growth. We observed a substantial reduction in the growth rate of the Δ*tolC* strain at 1 μM HCT, whereas WT growth remained unaffected (fig. S3). Differences in growth rate complicate quantitative comparisons of intracellular fluorescence between WT and Δ*tolC*. For example, different growth rates mean different rates of cell volume increase, hence different dilution rates of intracellular drug molecules, which can alter steady-state intracellular drug concentrations (*41*). The alteration in the intracellular drug concentration can, in turn, affect the growth rate, forming a feedback loop (*38*, *42*–*44*), that adds complexity to the interpretation of steady-state fluorescence measurements.

To avoid these confounding effects, we instead adjusted the external HCT concentration in Δ*tolC* to match the intracellular fluorescence levels observed in WT, i.e., the same number of target-bound HCT molecules. Through titration (fig. S4), we found that 0.05 μM HCT in Δ*tolC* yielded an $F_s$ value closely matching that of WT cells treated with 1 μM HCT (Fig. 1, A and B), with no statistically significant difference (Fig. 1C). At this lower dose, Δ*tolC* growth was unaffected (fig. S3). This large reduction in the external concentrations (20-fold reduction, from 1 to 0.05 μM) required to achieve the same number of DNA-bound HCT molecules underscores an important role of the efflux pumps in drug resistance.

A natural explanation for this difference in the external concentrations is that, as HCT molecules enter the periplasmic space, the AcrAB-TolC system captures them and exports them to the extracellular space, thereby lowering the net flux into the cytoplasm. This idea can be formalized mathematically (Supplementary Text, section 1). Briefly, let $P_{inward}$ denote the effective permeability governing drug influx. The total influx of drug molecules is given by $P_{inward} \times C_{out}$. Deletion of *tolC* prevents the capture, allowing more drug molecules to reach the cytoplasm. In this event, lowering the external concentration $C_{out}$ by the same factor should restore the total influx rate to the same value.

Therefore, with this gatekeeping mechanism alone, once the external concentration decreased by 20-fold, intracellular HCT accumulation dynamics should be the same between WT and Δ*tolC*. However, we found that, although both strains eventually converge to the same steady-state value, their initial accumulation slopes differed substantially (Fig. 1, A to C).

We next analyzed the slopes to deduce a difference in effective $P_{inward}$ between WT and Δ*tolC*. We assumed that, once drug molecules enter the cells, their biochemical interactions with the intracellular targets are identical in WT and Δ*tolC* strains. With this assumption, the difference in the initial slope in drug accumulation is primarily governed by the total influx rate, $P_{inward} \times C_{out}$, as discussed above. As shown in Fig. 1D, the slope in WT is higher by 3.7-fold than in Δ*tolC*. Given that the external concentration differed by 20-fold, this implies that the efflux pumps effectively reduce $P_{inward}$ by 5.4-fold (= 20/3.7; see eq. S12 in Supplementary Text).

### The HCT-DNA complex is more stable in Δ*tolC* than in WT

This 5.4-fold reduction in $P_{inward}$ by efflux pumps not only underscores their gatekeeping role but also raises a question: Why was a 20-fold difference in external HCT concentration required to equalize intracellular levels between WT and Δ*tolC*? Further analysis of the accumulation kinetics, $F(t)$, offers a clue. Earlier, we assumed that, once drug molecules enter the cell, their interaction with intracellular targets should be identical in WT and Δ*tolC* strains. However, this assumption is challenged by the observation that the Δ*tolC* strain reached the steady state substantially later than WT (Fig. 1, A and B). Specifically, according to standard drug-target kinetics (Supplementary Text, section 2), the time required to reach a steady state is primarily governed by the unbinding rate, $k_{off}$, which quantifies how quickly the drug-target complex dissociates (*17*, *20*, *21*). On the basis of this argument, the slower approach to steady state in Δ*tolC* suggests a lower $k_{off}$, i.e., a more stable HCT-DNA complex.

To test this hypothesis, we directly measured $k_{off}$ using a washout experiment. We first allowed intracellular fluorescence to reach a steady-state level. As described above, WT and Δ*tolC* cells were exposed to external HCT concentrations differing by 20-fold, such that both strains exhibit a similar number of DNA-bound HCT molecules. Cells were then washed and transferred to HCT-free media, and the decline in intracellular fluorescence was monitored over time (Fig. 2A). This decline followed first-order kinetics (linear on a semilog scale). The decline was substantially slower in the Δ*tolC* strain (Fig. 2A). We determined $k_{off}$ from the slope of this decline, which shows that it is ~4-fold lower in Δ*tolC* relative to WT (Fig. 2B), consistent with our prediction.

This difference in unbinding rates can be interpreted in terms of drug-target complex lifetime, defined as the average time a drug molecule remains bound to its target and given by the inverse of $k_{off}$ (*17*, *45*). In WT cells, the HCT-DNA complex lifetime was 10.9 min, whereas in Δ*tolC*, it extended to 42.6 min. Therefore, the complex is more stable in the efflux-deficient strain.

We tested the robustness of our findings through several additional experiments. In our initial measurements, samples were taken at multiple time points from the same culture, meaning that different cells were imaged at each point. To confirm that the observed differences in $k_{off}$ were not due to population variability, we used time-lapse microscopy to monitor fluorescence decay in individual cells over time. These single-cell measurements yielded $k_{off}$ values consistent with the population-level data for both strains (fig. S5), demonstrating that the unbinding kinetics are representative at the single-cell level.

Next, we assessed whether $k_{off}$ depends on external HCT concentration. Across a range of doses, we found only minor variation in $k_{off}$, and the Δ*tolC* strain consistently exhibited a substantially lower unbinding rate than WT (fig. S6), indicating that this effect is largely independent of external drug concentration.

Last, we tested whether this efflux-dependent modulation of $k_{off}$ also occurs in other bacterial species. *P. aeruginosa* is another Gram-negative species known for its high efflux activity. We used the PAO1Δ6 (Δ*mexAB-oprM*, Δ*mexCD-oprJ*, Δ*mexEF-oprN*, Δ*mexJKL*, Δ*mexXY*, and Δ*triABC*) (*46*), in which six best-characterized major efflux pump systems are knocked out. This strain again displayed a substantially lower $k_{off}$ value compared to WT (Fig. 2C and fig. S7).

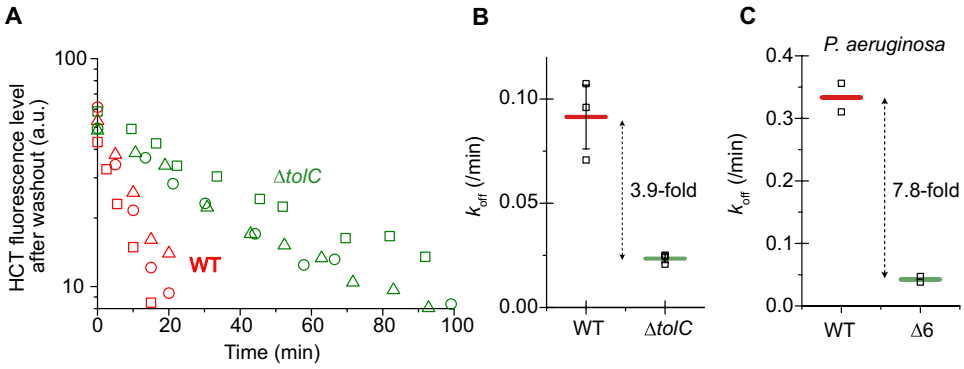


**Fig. 2. Decrease in intracellular HCT fluorescence intensity after HCT washout.** (**A**) After HCT washout, Δ*tolC* cells showed a slower decline in fluorescence than WT, indicating slower dissociation of HCT-DNA complexes. At least 30 cells were analyzed in each experiment. Three biological replicates were conducted (different symbols). (**B**) The slope of the fluorescence decline was analyzed to quantify the apparent $k_{off}$. It was ~4-fold lower in Δ*tolC* compared to WT. Open squares represent individual values from independent replicates. Horizontal bars and error bars indicate the means and SD from the replicates. (**C**) The same trend was observed in *P. aeruginosa*: The strain deficient in efflux pumps [PAO1Δ6 (*46*)] exhibited substantially lower $k_{off}$ values than WT (PAO1). This deficient strain lacks six major efflux pumps (Δ*mexAB-oprM*, Δ*mexCD-oprJ*, Δ*mexEF-oprN*, Δ*mexJKL*, Δ*mexXY*, and Δ*triABC*), whereas *mexGHI-opmD*, *mexVW*, *mexPQ-opmE*, *muxABC-ompB*, and *czcABCRS* and potentially other less characterized pumps remain intact.

Together, these results demonstrate that the impact of efflux pumps on intracellular drug-target unbinding kinetics is observable at the single-cell level, largely independent of drug concentration, and conserved across bacterial species—underscoring the robustness of our findings.

## A statistical mechanics model reveals that drug molecules frequently rebind to their targets in cells

The AcrAB-TolC efflux pumps are embedded in the bacterial envelope, whereas the HCT's target (DNA) resides in the cytoplasm. This spatial separation raises an important mechanistic question: How can efflux pumps influence the unbinding kinetics of drug-DNA complexes from a distance?

To explore this, we considered how the cellular environment might alter the fate of unbound drug molecules. In vitro measurements of $k_{off}$ are typically performed in dilute solutions, where drug molecules, after unbinding, diffuse away and are effectively lost to the bulk environment (*17*). In contrast, our measurements were conducted in cells, where diffusion occurs within a space bounded by the membrane. If the membrane were to behave as an absorbing boundary—removing any molecules that reach it—the fate of unbound drug molecules would resemble that of in vitro conditions.

Brownian motion of a diffusing particle in a sphere with a fully absorbing boundary is a classic problem in statistical physics. The average time a particle spends inside a sphere, the mean residence time τ, is given by (*47*)

$$\tau_a = \frac{R^2}{6D} \quad (1)$$

where $D$ is the diffusion coefficient of the particle and $R$ is the radius of a sphere. For small-molecule drugs (≲1 kDa) (*29*–*31*), $D$ generally lies in the range of $D = 10^0$ to $10^2$ μm$^2$/s (*48*, *49*). For this range of $D$, assuming $R = 1$ μm for a bacterial cell, $\tau_a$ is between 0.002 and 0.2 s. This implies that, if the cell membrane acts as a perfectly absorbing boundary, after a drug molecule unbinds from its target, it would be lost from the cell in under a second.

However, biological membranes do not behave as perfect sinks. Instead, they present a permeation barrier, reflecting a substantial fraction of diffusing molecules. Whether an intracellular molecule is reflected back into the cytoplasm or crosses the membrane into the extracellular space depends on membrane permeability. At higher permeability, more molecules escape the cell and are lost. At lower permeability, more molecules are reflected back, increasing their likelihood of remaining intracellular. As a result, the residence time of a unbound drug molecule within the cell τ will depend on the permeability, although it is expected to be higher than that under an idealized absorbing boundary condition ($\tau_a$).

To quantify this effect of the permeability on τ, we developed a statistical mechanics model of partially reflected Brownian motion (Supplementary Text, section 4). In this framework, particles diffuse within a confined compartment (e.g., a spherical bacterial cell) and encounter a boundary that probabilistically allows reflection or crossing, as defined by the Robin boundary condition (eq. S20). Reflected particles remain within the compartment, whereas those that cross are irreversibly lost.

We analytically solved this model and plotted the in-cell residence time τ, normalized by $\tau_a$, in Fig. 3A. This ratio quantifies how much longer an unbound molecule stays within a cell, relative to the fully absorbing boundary condition. This relative residence time decreases with increasing boundary permeability κ (Fig. 3A) because higher permeability increases the probability of escape. When κ exceeds ~10 μm/s, the ratio plateaus, indicating that the boundary behaves effectively as an absorbing surface (gray region in Fig. 3A).

A high $\tau/\tau_a$ ratio indicates that an intracellular drug molecule remains longer in the cell. A major consequence of this extended residence is an increased likelihood that unbound molecules reencounter their targets, resulting in repeated rebinding. To visualize the rebinding events, we expanded our model to incorporate drug-target interactions (Supplementary Text, section 5). We introduced a harmonic potential well within a spherical cell to represent the target site (i.e., nucleoid for HCT, denoted by the yellow area in Fig. 3B). Binding was modeled as a particle becoming trapped in the well, whereas unbinding occurred via spontaneous exit driven by thermal fluctuations.

Example trajectories (Fig. 3B) illustrate that, after exiting the potential well, particles frequently return to the target site via diffusion

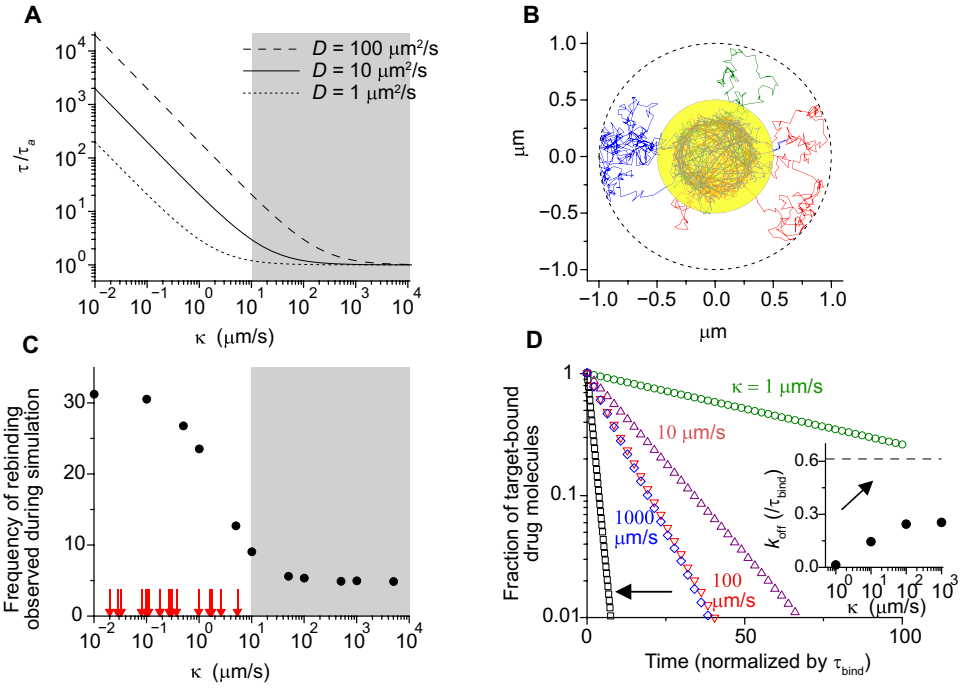


**Fig. 3. Statistical mechanics of partially reflected Brownian motion.** (**A**) Drug intracellular residence time $\tau$ in a spherical cell ($R = 1$ μm) as a function of boundary permeability κ (eq. S30), normalized by $\tau_a$ (fully absorbing boundary). See Supplementary Text for model details. The diffusion coefficient $D$ is typically in the range of $10^0$ to $10^2$ μm$^2$/s (*48*, *49*) for small-molecule drugs (≲1 kDa) (*29*–*31*). The gray shade indicates the region where the boundary behaves effectively as an absorbing surface. (**B**) A harmonic potential well at the center of a spherical cell (yellow region) represents the HCT intracellular target site, i.e., chromosomal DNA compacted into a nucleoid. On the basis of previous measurements (*65*, *66*), we set the radius of a nucleoid $R_{in} = 0.5$ μm. $D = 10$ μm$^2$/s and κ = 1 μm/s were used for simulations. The spring constant of the harmonic well was 800/s. With this constant, the average time that a particle takes to leave the potential well, $\tau_{bind}$, was 0.47 s (eq. S35). Typical trajectories show that particles that leave the well repeatedly return to the well. (**C**) Average number of times that a particle returns to the target site after escaping during 20 s of simulation. A total of $10^5$ trajectories were analyzed. Red arrows indicate experimentally measured membrane permeabilities of various drug molecules compiled from the literature (table S1). (**D**) To simulate an unbinding experiment, particles were initialized in the central potential well representing fully bound drug-target complexes. The number of particles remaining in the well was tracked over time at various boundary permeabilities κ. The time is normalized by $\tau_{bind}$. An arrow indicates a control simulation where rebinding was disabled—i.e., particles were not allowed to return to the potential well once escaped. Inset: Apparent $k_{off}$, extracted from the slope of the decay curves. The dashed line indicates $k_{off}^{intc}$ from the control simulation.

and become retrapped, demonstrating that drug molecules undergo repeated rebinding following unbinding. Because rebinding is mediated by diffusion, it occurs rapidly, on a timescale comparable to that required for a molecule to traverse the cell volume (fig. S8). We quantified the rebinding frequency—the number of times a unbound molecule returns to the target after initially escaping. As expected, increasing the diffusion coefficient led to more frequent rebinding (fig. S9A).

We next investigated the effects of boundary permeability κ on rebinding frequency. Above, we observed a higher $\tau/\tau_a$ ratio at lower permeability, indicating that drug molecules remain longer in the cell (Fig. 3A). This extended residence time leads to more frequent rebinding events (Fig. 3C). Conversely, when κ increases, rebinding frequency decreases, reaching a plateau when the boundary effectively behaves as an absorbing surface (gray zone in Fig. 3C).

To assess the relevance of these findings, we surveyed published measurements of membrane permeability for various small-molecule drugs in the literature (table S1). These values, shown as red arrows in Fig. 3C, all fall below 10 μm/s—well within the regime of frequent rebinding (to the left of the gray region). This suggests that rebinding is a common feature of drug molecules in cellular environments.

In summary, these simulations highlight a kinetic competition at the core of the rebinding process; intracellular diffusion favors the return of unbound molecules to their targets, whereas membrane permeation promotes escape and irreversible loss. Most small-molecule drugs exhibit high diffusion coefficients ($D = 10^0$ to $10^2$ μm$^2$/s) (*48*, *49*) but low permeability (table S1), resulting in frequent rebinding.

## Our model predicts important effects of rebinding on $k_{off}$

We next investigated how rebinding influences experimentally measured $k_{off}$ (i.e., apparent $k_{off}$). In washout experiments, $k_{off}$ is determined by first saturating the target sites with drug molecules and then monitoring a decline in target-bound molecules due to unbinding. However, frequent rebinding of unbound molecules (Fig. 3C), occurring on short timescales (fig. S8), can slow this decline, altering $k_{off}$.

To quantify this effect, we computationally simulated $k_{off}$ measurements. We initialized all particles in the central potential well, representing target-bound drug molecules. We then tracked the number of particles remaining trapped in the well over time, which exhibited a first-order decay (Fig. 3D). We extracted the apparent $k_{off}$ from the slope of this decay (Fig. 3D inset). As predicted, at low permeabilities—where rebinding is frequent—the number of particles

in the well declined slowly, leading to a lower $k_{off}$ (Fig. 3D). Conversely, as the boundary permeability κ increased, which suppresses rebinding (Fig. 3C), the apparent $k_{off}$ increased (Fig. 3D).

To isolate the effect of rebinding, we ran control simulations where particles were not allowed to reenter the potential well after escape. The resulting intrinsic unbinding rate, $k_{off}^{intc}$, is independent of rebinding, representing the thermodynamic stability of the drug-target complex. This intrinsic rate (dashed line and arrow in Fig. 3D) was substantially higher than the apparent $k_{off}$. Collectively, these simulation results demonstrate that rebinding substantially reduces the observed unbinding rate in cellular environments.

## Experimental tests of rebinding

The $k_{off}^{intc}$ is an intrinsic property determined by the thermodynamic stability of drug-target complexes (*19*, *20*). However, our model shows that, in the cellular context, when drug molecules unbind from their targets, they frequently return and rebind, causing $k_{off}$ to deviate from the intrinsic unbinding rate, $k_{off}^{intc}$. Our model also provides insight into how efflux pumps influence this deviation. Efflux pumps facilitate the export of intracellular drug molecules (*4*). This facilitated export, effectively acting as increasing the permeability for intracellular molecules, should reduce the in-cell residence time of drug molecules and hence their rebinding (Fig. 3, A to C), increasing the apparent $k_{off}$ (Fig. 3D).

We sought to test this model prediction by quantifying $k_{off}^{intc}$ and comparing it to the apparent $k_{off}$. Our experimental design was motivated by our simulation, where $k_{off}^{intc}$ was obtained by initializing particles in the potential well and preventing their return after unbinding (Fig. 3D). In experiments analogous to this simulation, cells were first preloaded with HCT such that DNA was initially bound by HCT. To prevent HCT rebinding, we subsequently added an excess of netropsin (NET), a DNA-targeting drug that occupies the same minor groove sites as HCT (*50*). As a result, the DNA sites vacated by unbinding HCT will be rapidly occupied by NET. This prevents HCT rebinding, enabling us to experimentally quantify $k_{off}^{intc}$.

We observed a substantially faster HCT fluorescence decay in the presence of excess NET (fig. S10), compared to our previous measurements in the absence of NET (Fig. 2). The slope of this decay, $k_{off}^{intc}$, was much higher than the previously observed $k_{off}$ (compare Fig. 4A and Fig. 2B), confirming that the apparent unbinding rate deviates from its intrinsic rate in the cell. $k_{off}^{intc}$ was nearly identical in WT and Δ*tolC E. coli* strains (Fig. 4A), indicating that the efflux did not alter the thermodynamic stability of the HCT-DNA complex.

We observed the same trend in *P. aeruginosa*; HCT fluorescence decayed more rapidly in the presence of NET (compare figs. S11 and S7). $k_{off}^{intc}$ was markedly higher than the apparent $k_{off}$ (compare Fig. 2C and Fig. 4C). In particular, $k_{off}^{intc}$ was similar between WT and Δ6 strains (Fig. 4C).

We next determined the degree of rebinding in efflux-active and efflux-deficient cells. We have observed in our computer simulation that rebinding causes the deviation of apparent $k_{off}$ from $k_{off}^{intc}$ (Fig. 3D). We mathematically formulated the relationship between this deviation and rebinding probability (eq. S18). Then, inserting the measured values of $k_{off}$ and $k_{off}^{intc}$ (Figs. 2, B and C, and 4, A and C) into this equation, we quantified the rebinding probability. The probability was lower in efflux-active strains than in their efflux-deficient counterparts, in both *E. coli* and *P. aeruginosa* (Fig. 4, B and D), confirming our model prediction that efflux pumps suppress rebinding.

## Differences in $k_{off}$ result in different drug-target affinities

Another often-cited parameter of drug efficacy is the drug-target binding affinity, quantified as an equilibrium dissociation constant $K_D$ (*17*). $K_D$ is equal to the ratio of the unbinding and binding rates, $K_D = k_{off}/k_{on}$. Therefore, any change in $k_{off}$ should directly influence the drug-target affinity inside the cell. In particular, a higher $k_{off}$ in efflux-active strains relative to efflux-deficient strains (Fig. 2) should lead to a higher $K_D$, indicating weaker binding affinity.

Although $K_D$ could be deduced from the kinetic constants ($k_{off}$ and $k_{on}$), it can also be quantified independently of them by measuring the ligand-receptor complex concentrations at the steady state against ligand concentrations, where the $K_D$ equals 50% of the maximum response (*17*). We measured the HCT-DNA $K_D$ through this independent approach. Intracellular HCT fluorescence intensity indicates the concentration of DNA-bound HCT molecules. We measured the steady-state intensity $F_s$ across a range of external HCT concentrations (fig. S12). The dose-response curve was well explained



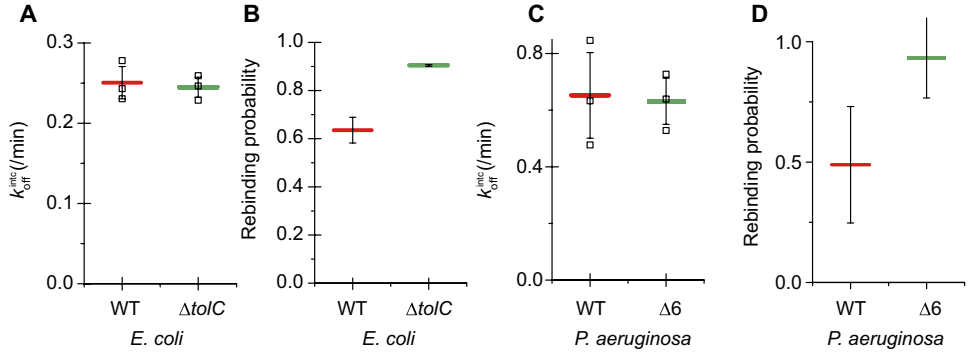


**Fig. 4. Efflux pumps modulate apparent unbinding rates by suppressing drug-target rebinding.** (**A**) Measurement of the intrinsic unbinding rate $k_{off}^{intc}$ of the HCT-DNA complex. Cells were preloaded with HCT to saturate DNA sites and then exposed to excess NET, a competitive DNA binding molecule, to block HCT rebinding after washout. HCT fluorescence decay was monitored over time (fig. S10), and $k_{off}^{intc}$ was determined from the slope of the decay. No substantial difference was observed between WT and Δ*tolC* strains, confirming that efflux pumps do not alter the intrinsic chemical stability of the HCT-DNA complex. (**B**) Rebinding probability, deduced from the deviation of the apparent $k_{off}$ (measured without NET) from intrinsic $k_{off}^{intc}$ (measured with NET) using eq. S18. The Δ*tolC* strain exhibited a substantially higher rebinding probability than WT. (**C** and **D**) $k_{off}^{intc}$ and rebinding probability in *P. aeruginosa*. Open squares represent individual values from independent replicates. Horizontal bars and error bars indicate the means and SD from the replicates.

by a standard binding model, which we then fit to extract the apparent $K_D$ (fig. S12).

We found that the apparent $K_D$ was ~4.5-fold lower in Δ*tolC* cells compared to WT (fig. S12), closely matching the ~4-fold difference in $k_{off}$ between these two strains (Fig. 2B). Given that $K_D = k_{off}/k_{on}$, this match suggests that the observed increase in the apparent binding affinity in Δ*tolC* arises primarily from the reduction in unbinding rate, rather than changes in the association rate. Collectively, our data indicate that efflux pumps affect the drug-target equilibrium constant (apparent affinity) by altering the unbinding kinetics, mediated through a change in rebinding frequency.

## DISCUSSION

Drug-target interactions, characterized by their binding affinity and kinetic rates, are central to determining drug efficacy (*17*, *20*). In our study, we observed that efflux-active cells exhibit a lower apparent drug-target affinity and higher apparent unbinding rate, i.e., weaker drug-target interactions, than efflux-deficient cells. Following the common explanation in in vitro studies, we had initially considered whether this effect was due to altered thermodynamic stability of drug-target complexes. However, our direct measurements of the intrinsic unbinding rate, $k_{off}^{intc}$, confirmed that the thermodynamics of their interactions remain unchanged (Fig. 4). Instead, our in-depth live-cell measurements and statistical mechanics–based modeling revealed that drug-target interactions in the cellular environments are stabilized by rapid rebinding of drug molecules. Efflux pumps limit rebinding by removing unbound drug molecules from the cell, thereby destabilizing drug-target interactions through a kinetic—not thermodynamic—mechanism.

This finding uncovers a previously unrecognized mode of efflux-mediated resistance. For a drug to be intracellularly functional, it must not only enter the cell but also occupy its targets. Any impediments to either (i) drug entry or (ii) target occupation contribute to drug resistance (*2*). Efflux pumps are well known for their "gatekeeping" role in limiting drug entry. Consistent with this, we observed that they reduce intracellular HCT accumulation by ~5-fold (Fig. 1 and eq. S12). The focus of this study was on the latter, demonstrating that efflux pumps remotely reduce target occupation. This reduction is mediated by rapid removal of unbound molecules, suppressing rebinding and increasing the apparent $k_{off}$. On the other hand, in efflux-deficient strains, unbound molecules diffuse around in the cells longer, which results in frequent rebinding and lower apparent $k_{off}$. We found that this "housekeeping" mechanism increased the apparent HCT-DNA unbinding rate by ~4-fold and the apparent affinity by a similar degree (Fig. 2 and fig. S12).

This fivefold restriction in HCT entry and fourfold reduction in the apparent affinity together explains why a 20-fold (= 5 × 4) higher external HCT concentration was required in WT cells to achieve the same level of target occupancy to that of Δ*tolC* (Fig. 1, A to C). Thus, efflux pumps do not merely block drug entry—they actively reshape intracellular drug-target interactions. Fully understanding their impact requires accounting for these two functions, underscoring the multifaceted and dynamic nature of efflux-mediated drug resistance.

This housekeeping mechanism requires transport of substrates from the cytoplasm to the extracellular space. Although the favored view is that AcrAB-TolC primarily captures substrates in the periplasm (*13*, *14*), structural studies have suggested AcrB could also allow capture from the inner leaflet of the inner membrane or directly from the cytoplasm (*10*, *11*, *51*). Other RND transporters have been shown to acquire substrates from the cytoplasm [e.g., AcrAD-TolC (*52*, *53*), CusCBA (*54*), and CzcCBA (*55*)]. Furthermore, efflux pumps from other families can move substrates from the cytoplasm into the periplasm (*56*, *57*). Thus, even if AcrAB-TolC itself might primarily act on periplasmic substrates, it can still contribute to the removal of cytoplasmic molecules through cooperative action with other pumps. These various processes ensure that efflux contributes broadly to the removal of intracellular molecules.

It is also important to note that the cytoplasm is a crowded medium rather than a dilute solution; macromolecular crowding affects the effective diffusion constant of small molecules, reduces their accessible volumes, increases the target search time, and promotes nonspecific interactions (*49*, *58*, *59*), which could additionally alter rebinding dynamics.

Our quantitative analysis provides an important mechanistic insight into this housekeeping function. Most drugs are small molecules (≲1 kDa) (*29*–*31*), with the diffusion constant generally in the range of $D = 10^0$ to $10^2$ μm$^2$/s (*48*, *49*). The diffusion constant determines the time a molecule needs to traverse the cytoplasm, which is equivalent to $\tau_a$ in Eq. 1. Another critical factor shaping rebinding is the timescale for a molecule to exit the cell via permeation ($\tau_P$). The balance between intracellular diffusion ($\tau_a$) and permeation ($\tau_P$) determines the likelihood of rebinding. If $\tau_P < \tau_a$, molecules rapidly exit the cells, and thus rebinding is rare. By contrast, when $\tau_P > \tau_a$, molecules traverse the intracellular volume multiple times before leaving, leading to frequent rebinding. This is the regime where efflux pumps can suppress rebinding to modulate the apparent $k_{off}$. For example, with $D = 10$ μm$^2$/s, the time to diffuse across an *E. coli* cell (approximated as a sphere with radius $R = 1$ μm) is on the order of tens of milliseconds (Eq. 1). The corresponding permeation time can be estimated as $\tau_P \approx V/(A \times P)$, where $P$ is the membrane permeability, $V$ is the cell volume, and $A$ is the cell surface area. To enter the rebinding-favorable regime ($\tau_P > \tau_a$), the permeability must be on the order of tens of micrometers per second or lower. Our simulations confirm that rebinding frequency rises steeply in this regime as permeability decreases (Fig. 3, C and D). Furthermore, published measurements of membrane permeabilities for diverse small-molecule drugs fall within this regime of increasing rebinding frequency (table S1; red arrows in Fig. 3C). This overlap indicates that efflux pumps are well poised to limit drug-target rebinding in the cell across a broad spectrum of drug molecules. Coupled with their broad substrate specificity—particularly those of the RND family (*7*)—this finding provides physical insights into how efflux pumps contribute broadly to multidrug resistance.

These insights also have important implications for understanding drug action and designing new therapeutics. Although extensive efforts have focused on optimizing the thermodynamic properties of drug-target interactions (*21*, *60*), the accessible chemical space for such optimization is not infinite. This work underscores the importance of spatial constraints and kinetic factors in intact cells—such as intracellular diffusion, membrane permeability, and efflux activity—in shaping drug efficacy. Efflux activity can be inhibited directly (*16*), membrane permeability may be modulated by adjuvants (*61*), and the effective intracellular diffusion coefficient could be influenced indirectly, e.g., by designing molecules with reduced nonspecific binding ("less sticky") to cytoplasmic components. By targeting these factors, it may be possible to enhance drug performance, offering a complementary strategy for improving therapeutic outcomes.

## MATERIALS AND METHODS

### Bacterial strains and culture conditions

*E. coli* K-12 NCM3722 was used (*62*). Δ*tolC* was constructed using P1 transduction using Keio collection knockouts (*63*). *P. aeruginosa* strains PAO1 and PAO1Δ6 (*46*) (Δ*mexAB-oprM*, Δ*mexCD-oprJ*, Δ*mexEF-oprN*, Δ*mexJKL*, Δ*mexXY*, and Δ*triABC*) were gifts from the Graeme Conn lab (Emory University).

Cells were cultured in Neidhart Mops minimal media (*64*) with 10 mM glucose and 10 mM $NH_4Cl$ as the carbon and nitrogen sources.

To prepare experimental cultures, cells were taken from −80°C stocks and streaked on an LB plate. A single colony was inoculated in 2 ml of LB medium and grown at 37°C with constant agitation at 250 rpm in a water bath. To monitor growth, the optical density ($OD_{600}$) of the culture was measured using a Genesys20 spectrophotometer with a standard quartz cuvette. Before cells entered stationary phase, cells were inoculated into 5 ml of Mops minimal medium at very low densities (typically lower than the $OD_{600}$ of ~0.0001) and cultured overnight (preculture). The next morning, the preculture was diluted in the prewarmed, 3-ml Mops minimal medium (experimental culture) to the $OD_{600}$ of ~0.01 and allowed to grow exponentially.

### HCT measurements

HCT was purchased from Sigma-Aldrich. HCT was added to the exponentially growing culture at an OD of 0.05 at desired concentrations. Samples were taken at specified time points and placed on a microscope coverslip. A 1.5% agar pad containing the same medium composition as the culture was placed on the coverslip and transferred to the microscope stage.

Images were acquired using an Olympus inverted fluorescence microscope with a 60× oil lens. Fluorescence was taken with a 4′,6-diamidino-2-phenylindole (DAPI) filter set using a 500-ms exposure time. Bright-field images for identification of whole cells were captured at the same time using 200-ms exposure through the same filter cube and phase contrast illumination. At least 30 cells were imaged. Images were recorded using an Andor Neo 5.5 CMOS camera and analyzed using ImageJ. Thresholding was conducted on the phase contrast images to identify cells, creating a mask. This mask was then overlaid on the fluorescence images, and the average fluorescence was calculated.

In experiments to measure $k_{off}$, 1 and 0.05 mM HCT for *E. coli* (WT and Δ*tolC*) and 50 and 15 μM for *P. aeruginosa* (PAO1 and PAO1Δ6) were added to the culture and incubated for at least 30 min. The culture was then centrifuged at 2000*g* for 5 min, and the supernatant was replaced with fresh medium lacking HCT and centrifuged again to wash out any residual HCT. Samples were taken at specific time points and measured as described above.

To measure $k_{off}^{intc}$, a growing culture was inoculated with HCT at an $OD_{600}$ of 0.03 for 30 min. NET (5 μg/ml; Enzo Life Sciences) for *E. coli* and PAO1, NET (2.5 μg/ml) for *E. coli* Δ*tolC*, and NET (0.3 mg/ml) for PAO1Δ6 were added and incubated for 20 min. HCT was removed from the medium by centrifugation and replaced with NET-containing media.

### Simulation

We performed a Monte Carlo simulation in C++. The particle position was updated iteratively at each time step using eq. S33 within a spherical harmonic potential well and eq. S34 outside the potential well. The simulation space was confined within a spherical boundary of radius $R$. When the particle reached this boundary, whether it was absorbed or reflected was determined probabilistically using eq. S20, with the probability of absorption given by $\frac{\kappa}{D}dr$, where $\kappa$ is the permeability coefficient and $dr$ is the radial increment. If absorbed, the simulation for that particle was terminated; otherwise, the particle was reflected and repositioned within the boundary. The time step $\Delta t$ was selected to satisfy the stability condition $\sqrt{2D\Delta t} \leq 2 \times 10^{-8}$ m, ensuring that the particle's displacement remained within the smallest spatial resolution used, thereby maintaining numerical accuracy throughout the simulation. The force constant $k$ was set to 800 $s^{-1}$ throughout the simulation. This value was selected because it provides a balance where the average residence time of the particle within the harmonic potential well is neither too short nor too long. To ensure statistically robust estimates of key metrics such as the residence probability within the well, the return time distribution, and the frequency of rebinding events, we simulated $10^5$ independent particle trajectories. For a comprehensive description of the simulation framework and parameter choices, see sections 4 and 5 in Supplementary Text for details.

## Supplementary Materials

**The PDF file includes:**

Supplementary Text
Figs. S1 to S13
Table S1
Legend for data S1
Legend for code S1
References

**Other Supplementary Material for this manuscript includes the following:**

Data S1
Code S1

## REFERENCES


1. Antimicrobial Resistance Collaborators, Global burden of bacterial antimicrobial resistance in 2019: A systematic analysis. *Lancet* **399**, 629–655 (2022).
2. J. M. A. Blair, M. A. Webber, A. J. Baylay, D. O. Ogbolu, L. J. V. Piddock, Molecular mechanisms of antibiotic resistance. *Nat. Rev. Microbiol.* **13**, 42–51 (2015).
3. H. Nikaido, Multidrug resistance in bacteria. *Annu. Rev. Biochem.* **78**, 119–146 (2009).
4. K. Poole, Efflux pumps as antimicrobial resistance mechanisms. *Ann. Med.* **39**, 162–176 (2007).
5. I. El Meouche, M. J. Dunlop, Heterogeneity in efflux pump expression predisposes antibiotic-resistant cells to mutation. *Science* **362**, 686–690 (2018).
6. M. Putman, H. W. van Veen, W. N. Konings, Molecular properties of bacterial multidrug transporters. *Microbiol. Mol. Biol. Rev.* **64**, 672–693 (2000).
7. H. Nikaido, H. I. Zgurskaya, AcrAB and related multidrug efflux pumps of *Escherichia coli*. *J. Mol. Microbiol. Biotechnol.* **3**, 215–218 (2001).
8. L. J. Piddock, Clinically relevant chromosomally encoded multidrug resistance efflux pumps in bacteria. *Clin. Microbiol. Rev.* **19**, 382–402 (2006).
9. S. Jang, AcrAB-TolC, a major efflux pump in Gram negative bacteria: Toward understanding its operation mechanism. *BMB Rep.* **56**, 326–334 (2023).
10. S. Murakami, R. Nakashima, E. Yamashita, A. Yamaguchi, Crystal structure of bacterial multidrug efflux transporter AcrB. *Nature* **419**, 587–593 (2002).
11. E. W. Yu, G. McDermott, H. I. Zgurskaya, H. Nikaido, D. E. Koshland Jr., Structural basis of multiple drug-binding capacity of the AcrB multidrug efflux pump. *Science* **300**, 976–980 (2003).
12. Z. Wang, G. Fan, C. F. Hryc, J. N. Blaza, I. I. Serysheva, M. F. Schmid, W. Chiu, B. F. Luisi, D. Du, An allosteric transport mechanism for the AcrAB-TolC multidrug efflux pump. *eLife* **6**, e24905 (2017).
13. O. Lomovskaya, H. I. Zgurskaya, H. Nikaido, It takes three to tango. *Nat. Biotechnol.* **20**, 1210–1212 (2002).
14. P. A. Klenotic, E. W. Yu, Structural analysis of resistance-nodulation cell division transporters. *Microbiol. Mol. Biol. Rev.* **88**, e0019823 (2024).
15. H. I. Zgurskaya, G. Krishnamoorthy, A. Ntreh, S. Lu, Mechanism and Function of the outer membrane channel TolC in multidrug resistance and physiology of enterobacteria. *Front. Microbiol.* **2**, 189 (2011).

16. M. Duffey, R. P. Jumde, R. M. A. da Costa, H.-K. Ropponen, B. Blasco, L. J. V. Piddock, Extending the potency and lifespan of antibiotics: Inhibitors of Gram-negative bacterial efflux pumps. *ACS Infect. Dis.* **10**, 1458–1482 (2024).
17. S. Núñez, J. Venhorst, C. G. Kruse, Target–drug interactions: First principles and their application to drug discovery. *Drug Discov. Today* **17**, 10–22 (2012).
18. M. K. Gilson, H. X. Zhou, Calculation of protein-ligand binding affinities. *Annu. Rev. Biophys. Biomol. Struct.* **36**, 21–42 (2007).
19. A. C. Pan, D. W. Borhani, R. O. Dror, D. E. Shaw, Molecular determinants of drug–receptor binding kinetics. *Drug Discov. Today* **18**, 667–673 (2013).
20. R. A. Copeland, D. L. Pompliano, T. D. Meek, Drug–target residence time and its implications for lead optimization. *Nat. Rev. Drug Discov.* **5**, 730–739 (2006).
21. M. Bernetti, M. Masetti, W. Rocchia, A. Cavalli, Kinetics of drug binding and residence time. *Annu. Rev. Phys. Chem.* **70**, 143–171 (2019).
22. M. B. Robers, R. Friedman-Ohana, K. V. M. Huber, L. Kilpatrick, J. D. Vasta, B.-T. Berger, C. Chaudhry, S. Hill, S. Müller, S. Knapp, K. V. Wood, Quantifying target occupancy of small molecules within living cells. *Annu. Rev. Biochem.* **89**, 557–581 (2020).
23. R. D. Taylor, M. MacCoss, A. D. Lawson, Rings in drugs. *J. Med. Chem.* **57**, 5845–5859 (2014).
24. Y. Bansal, O. Silakari, The therapeutic journey of benzimidazoles: A review. *Bioorg. Med. Chem.* **20**, 6208–6236 (2012).
25. J. B. Wright, The chemistry of the benzimidazoles. *Chem. Rev.* **48**, 397–541 (1951).
26. S. Tahlan, S. Kumar, B. Narasimhan, Pharmacological significance of heterocyclic 1*H*-benzimidazole scaffolds: A review. *BMC Chem.* **13**, 101 (2019).
27. J. Bucevičius, G. Lukinavičius, R. Gerasimaitė, The use of Hoechst dyes for DNA staining and beyond. *Chemosensors* **6**, 18 (2018).
28. A. Daina, O. Michielin, V. Zoete, SwissADME: A free web tool to evaluate pharmacokinetics, drug-likeness and medicinal chemistry friendliness of small molecules. *Sci. Rep.* **7**, 42717 (2017).
29. P. D. Leeson, B. Springthorpe, The influence of drug-like concepts on decision-making in medicinal chemistry. *Nat. Rev. Drug Discov.* **6**, 881–890 (2007).
30. U. Fagerholm, Investigation of Molecular Weights and Pharmacokinetic Characteristics of Older and Modern Small. bioRxiv 508888 [Preprint] (2022). https://doi.org/10.1101/2022.09.21.508888.
31. A. Johnson, *Antimicrobial Agents: Antibacterials and Antifungals*, A. Bryskier, Ed. (ASM Press, 2005), pp. 1456.
32. B. M. Swain, D. Guo, H. Singh, P. B. Rawlins, M. McAlister, H. W. van Veen, Complexities of a protonatable substrate in measurements of Hoechst 33342 transport by multidrug transporter LmrP. *Sci. Rep.* **10**, 20026 (2020).
33. P. G. Baraldi, A. Bovero, F. Fruttarolo, D. Preti, M. A. Tabrizi, M. G. Pavani, R. Romagnoli, DNA minor groove binders as potential antitumor and antimicrobial agents. *Med. Res. Rev.* **24**, 475–528 (2004).
34. H. Nikaido, Multidrug efflux pumps of gram-negative bacteria. *J. Bacteriol.* **178**, 5853–5859 (1996).
35. J. M. A. Blair, L. J. V. Piddock, How to measure export via bacterial multidrug resistance efflux pumps. *mBio* **7**, e00840 (2016).
36. J. Bontemps, C. Houssier, E. Fredericq, Physico-chemical study of the complexes of "33258 Hoechst" with DNA and nucleohistone. *Nucleic Acids Res.* **2**, 971–984 (1975).
37. B. Weisblum, E. Haenssler, Fluorometric properties of the bibenzimidazole derivative Hoechst 33258, a fluorescent probe specific for AT concentration in chromosomal DNA. *Chromosoma* **46**, 255–260 (1974).
38. D. Le, T. Akiyama, D. Weiss, M. Kim, Dissociation kinetics of small-molecule inhibitors in *Escherichia coli* is coupled to physiological state of cells. *Commun. Biol.* **6**, 223 (2023).
39. H. Sjuts, A. V. Vargiu, S. M. Kwasny, S. T. Nguyen, H.-S. Kim, X. Ding, A. R. Ornik, P. Ruggerone, T. L. Bowlin, H. Nikaido, K. M. Pos, T. J. Opperman, Molecular basis for inhibition of AcrB multidrug efflux pump by novel and powerful pyranopyridine derivatives. *Proc. Natl. Acad. Sci. U.S.A.* **113**, 3509–3514 (2016).
40. T. J. Opperman, S. M. Kwasny, H. S. Kim, S. T. Nguyen, C. Houseweart, S. D'Souza, G. C. Walker, N. P. Peet, H. Nikaido, T. L. Bowlin, Characterization of a novel pyranopyridine inhibitor of the AcrAB efflux pump of *Escherichia coli*. *Antimicrob. Agents Chemother.* **58**, 722–733 (2014).
41. P. Abel, zur Wiesch, S. Abel, S. Gkotzis, P. Ocampo, J. Engelstädter, T. Hinkley, C. Magnus, M. K. Waldor, K. Udekwu, T. Cohen, Classic reaction kinetics can explain complex patterns of antibiotic action. *Sci. Transl. Med.* **7**, 287ra73 (2015).
42. B. Deris, M. Kim, Z. Zhang, H. Okano, R. Hermsen, A. Groisman, T. Hwa, The innate growth bistability of antibiotic resistant bacteria. *Science* **342**, 1237435 (2013).
43. C. Tan, P. Marguet, L. You, Emergent bistability by a growth-modulating positive feedback circuit. *Nat. Chem. Biol.* **5**, 842–848 (2009).
44. J. Elf, K. Nilsson, T. Tenson, M. Ehrenberg, Bistable bacterial growth rate in response to antibiotics with low membrane permeability. *Phys. Rev. Lett.* **97**, 258104 (2006).
45. P. Tiwary, V. Limongelli, M. Salvalaglio, M. Parrinello, Kinetics of protein–ligand unbinding: Predicting pathways, rates, and rate-limiting steps. *Proc. Natl. Acad. Sci. U.S.A.* **112**, E386–E391 (2015).
46. J. W. Adamiak, V. Jhawar, V. Bonifay, C. E. Chandler, I. V. Leus, R. K. Ernst, H. P. Schweizer, H. I. Zgurskaya, Loss of RND-type multidrug efflux pumps triggers iron starvation and lipid A modifications in *Pseudomonas aeruginosa*. *Antimicrob. Agents Chemother.* **65**, e0059221 (2021).
47. N. Agmon, Residence times in diffusion processes. *J. Chem. Phys.* **81**, 3644–3647 (1984).
48. J. T. Mika, G. Van Den Bogaart, L. Veenhoff, V. Krasnikov, B. Poolman, Molecular sieving properties of the cytoplasm of *Escherichia coli* and consequences of osmotic stress. *Mol. Microbiol.* **77**, 200–207 (2010).
49. J. T. Mika, B. Poolman, Macromolecule diffusion and confinement in prokaryotic cells. *Curr. Opin. Biotechnol.* **22**, 117–126 (2011).
50. M. Poot, K. Kausch, J. Köhler, T. Haaf, H. Hoehn, The minor-groove binding DNA-ligands netropsin, distamycin A and berenil cause polyploidisation via impairment of the G2 phase of the cell cycle. *Cell Struct. Funct.* **15**, 151–157 (1990).
51. M. A. Seeger, A. Schiefner, T. Eicher, F. Verrey, K. Diederichs, K. M. Pos, Structural asymmetry of AcrB trimer suggests a peristaltic pump mechanism. *Science* **313**, 1295–1298 (2006).
52. J. R. Aires, H. Nikaido, Aminoglycosides are captured from both periplasm and cytoplasm by the AcrD multidrug efflux transporter of *Escherichia coli*. *J. Bacteriol.* **187**, 1923–1929 (2005).
53. Z. Zhang, C. E. Morgan, M. Cui, E. W. Yu, Cryo-EM structures of AcrD illuminate a mechanism for capturing aminoglycosides from its central cavity. *mBio* **14**, e0338322 (2023).
54. F. Long, C. C. Su, M. T. Zimmermann, S. E. Boyken, K. R. Rajashankar, R. L. Jernigan, E. W. Yu, Crystal structures of the CusA efflux pump suggest methionine-mediated metal transport. *Nature* **467**, 484–488 (2010).
55. M. Goldberg, T. Pribyl, S. Juhnke, D. H. Nies, Energetics and topology of CzcA, a cation/proton antiporter of the resistance-nodulation-cell division protein family. *J. Biol. Chem.* **274**, 26065–26070 (1999).
56. M. Palmer, Efflux of cytoplasmically acting antibiotics from gram-negative bacteria: Periplasmic substrate capture by multicomponent efflux pumps inferred from their cooperative action with single-component transporters. *J. Bacteriol.* **185**, 5287–5289 (2003).
57. N. Tal, S. Schuldiner, A coordinated network of transporters with overlapping specificities provides a robust survival strategy. *Proc. Natl. Acad. Sci. U.S.A.* **106**, 9051–9056 (2009).
58. H.-X. Zhou, G. Rivas, A. P. Minton, Macromolecular crowding and confinement: Biochemical, biophysical, and potential physiological consequences. *Annu. Rev.Biophys.* **37**, 375–397 (2008).
59. L. Liu, K. Luo, Molecular crowding effect on dynamics of DNA-binding proteins search for their targets. *J. Chem. Phys.* **141**, 225102 (2014).
60. P. J. Tonge, Drug–target kinetics in drug discovery. *ACS Chem. Neurosci.* **9**, 29–39 (2018).
61. G. Dhanda, Y. Acharya, J. Haldar, Antibiotic adjuvants: A versatile approach to combat antibiotic resistance. *ACS Omega* **8**, 10757–10783 (2023).
62. E. Soupene, W. C. van Heeswijk, J. Plumbridge, V. Stewart, D. Bertenthal, H. Lee, G. Prasad, O. Paliy, P. Charernnoppakul, S. Kustu, Physiological studies of *Escherichia coli* strain MG1655: Growth defects and apparent cross-regulation of gene expression. *J. Bacteriol.* **185**, 5611–5626 (2003).
63. T. Baba, T. Ara, M. Hasegawa, Y. Takai, Y. Okumura, M. Baba, K. A. Datsenko, M. Tomita, B. L. Wanner, H. Mori, Construction of *Escherichia coli* K-12 in-frame, single-gene knockout mutants: The Keio collection. *Mol. Syst. Biol.* **2**, 2006.0008 (2006).
64. F. C. Neidhardt, P. L. Bloch, D. F. Smith, Culture medium for enterobacteria. *J. Bacteriol.* **119**, 736–747 (1974).
65. M.-H. Chang, M. O. Lavrentovich, J. Männik, Differentiating the roles of proteins and polysomes in nucleoid size homeostasis in *Escherichia coli*. *Biophys. J.* **123**, 1435–1448 (2024).
66. S. Bakshi, A. Siryaporn, M. Goulian, J. C. Weisshaar, Superresolution imaging of ribosomes and RNA polymerase in live *Escherichia coli* cells. *Mol. Microbiol.* **85**, 21–38 (2012).
67. D. A. Westfall, G. Krishnamoorthy, D. Wolloscheck, R. Sarkar, H. I. Zgurskaya, V. V. Rybenkov, Bifurcation kinetics of drug uptake by Gram-negative bacteria. *PLOS ONE* **12**, e0184671 (2017).
68. G. Youlden, H. E. McNeil, J. M. A. Blair, S. Jabbari, J. R. King, Mathematical modelling highlights the potential for genetic manipulation as an adjuvant to counter efflux-mediated MDR in Salmonella. *Bull. Math Biol.* **84**, 56 (2022).
69. W. W. Nichols, Modeling the kinetics of the permeation of antibacterial agents into growing bacteria and its interplay with efflux. *Antimicrob. Agents Chemother.* **61**, e02576–e02516 (2017).
70. C. Gardiner, *Stochastic Methods: A Handbook for the Natural and Social Sciences* (Springer Berlin Heidelberg, 2010).
71. H. Kersting, A. Orvieto, F. Proske, A. Lucchi, Mean first exit times of Ornstein–Uhlenbeck processes in high-dimensional spaces. *J. Phys. A Math. Theor.* **56**, 215003 (2023).
72. F. R. Blattner, G. Plunkett, C. A. Bloch, N. T. Perna, V. Burland, The complete genome sequence of *Escherichia coli* K-12. *Science* **277**, 1453–1462 (1997).

73. L. Goracci, R. Germani, G. Savelli, D. M. Bassani, Hoechst 33258 as a pH-sensitive probe to study the interaction of amine oxide surfactants with DNA. *Chembiochem* **6**, 197–203 (2005).
74. T. R. Downs, W. W. Wilfinger, Fluorometric quantification of DNA in cells and tissue. *Anal. Biochem.* **131**, 538–547 (1983).
75. N. Matsumura, S. Minami, Y. Watanabe, S. Iyobe, S. Mitsuhashi, Role of permeability in the activities of β-lactams against gram-negative bacteria which produce a group 3 β-lactamase. *Antimicrob. Agents Chemother.* **43**, 2084–2086 (1999).
76. S. Kojima, H. Nikaido, Permeation rates of penicillins indicate that *Escherichia coli* porins function principally as nonspecific channels. *Proc. Natl. Acad. Sci. U.S.A.* **110**, E2629–E2634 (2013).
77. H. Nikaido, S. Normark, Sensitivity of *Escherichia coli* to various β-lactams is determined by the interplay of outer membrane permeability and degradation by periplasmic β-lactamases: A quantitative predictive treatment. *Mol. Microbiol.* **1**, 29–36 (1987).
78. H. Nikaido, E. Y. Rosenberg, J. Foulds, Porin channels in *Escherichia coli*: Studies with beta-lactams in intact cells. *J. Bacteriol.* **153**, 232–240 (1983).
79. W. Liu, H. Nikaido, Contribution of the cell-surface-associated enzyme in the Zimmermann-Rosselet assay of outer membrane permeability of beta-lactam antibiotics. *Antimicrob. Agents Chemother.* **35**, 177–179 (1991).


**Acknowledgments:** We thank G. Conn for sharing the *P. aeruginosa* strain deficient in efflux pumps (PAO1Δ6). **Funding:** We acknowledge support from the National Institutes of Health (U19AI158080 to S.D., K.S., D.L., and M.K.). **Author contributions:** S.D.: Conceptualization, investigation, writing—review and editing, methodology, resources, data curation, validation, formal analysis, software, and visualization. K.S.: Conceptualization, investigation, writing—review and editing, methodology, resources, data curation, validation, and software. D.L.: Conceptualization, Investigation, methodology, data curation, validation, formal analysis, and visualization. M.K.: Writing—original draft, conceptualization, investigation, writing—review and editing, resources, funding acquisition, validation, supervision, formal analysis, project administration, and visualization. **Competing interests:** The authors declare that they have no competing interests. **Data and materials availability:** All data and code needed to evaluate and reproduce the results in the paper are present in the paper and/or the Supplementary Materials.

Submitted 22 July 2025
Accepted 31 December 2025
Published 28 January 2026
10.1126/sciadv.aea7983

ScienceAdvances

# Efflux pumps control intracellular drug-target kinetics by limiting rebinding in bacteria

Subrata Dev, Keiran Stevenson, Dai Le, and Minsu Kim

*Sci. Adv.* **12** (5), eaea7983. DOI: 10.1126/sciadv.aea7983



*Science Advances* (ISSN 2375-2548) is published by the American Association for the Advancement of Science. 1200 New York Avenue NW, Washington, DC 20005. The title *Science Advances* is a registered trademark of AAAS.